# MIT Open Access Articles

## Multiplexed Single-Cell Leukocyte Enzymatic Secretion Profiling from Whole Blood Reveals Patient-Specific Immune Signature

**Massachusetts Institute of Technology**

Article

# Multiplexed Single-Cell Leukocyte Enzymatic Secretion Profiling from Whole Blood Reveals Patient-Specific Immune Signature

Kerwin Kwek Zeming,* Ri Lu, Kai Lee Woo, Guoyun Sun, Kai Yun Quek, Lih Feng Cheow, Chia-Hung Chen, Jongyoon Han, and Shir Lynn Lim*

Read Online

ACCESS | Metrics & More | Article Recommendations | Supporting Information

**ABSTRACT:** Enzymatic secretion of immune cells (leukocytes) plays a dominant role in host immune responses to a myriad of biological triggers, including infections, cancers, and cardiovascular diseases. Current tools to probe these leukocytes inadequately profile these vital biomarkers; the need for sample preprocessing steps of cell lysis, labeling, washing, and pipetting inevitably triggers the cells, changes its basal state, and dilutes the individual cell secretion in bulk assays. Using a fully integrated system for multiplexed profiling of native immune single-cell enzyme secretion from 50 $\mu$L of undiluted blood, we eliminate sample handling. With a total analysis time of 60 min, the integrated platform performs six tasks of leukocyte extraction, cell washing, fluorescent enzyme substrate mixing, single-cell droplet making, droplet incubation, and real-time readout for leukocyte secretion profiling of neutrophil elastase, granzyme B, and metalloproteinase. We calibrated the device, optimized the protocols, and tested the leukocyte secretion of acute heart failure (AHF) patients at admission and predischarge. This paper highlights the presence of single-cell enzymatic immune phenotypes independent of CD marker labeling, which could potentially elucidate the innate immune response states. We found that patients recovering from AHF showed a corresponding reduction in immune-cell enzymatic secretion levels and donor-specific enzymatic signatures were observed, which suggests patient-to-patient heterogeneous immune response. This platform presents opportunities to elucidate the complexities of the immune response from a single drop of blood and bridge the current technological, biological, and medical gap in understanding immune response and biological triggers.
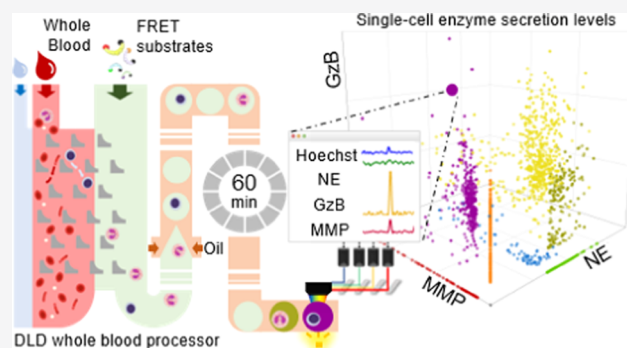
## INTRODUCTION

Human immune response is an ever-vigilant and dynamic system designed to resolve intrinsic and extrinsic triggers such as cancers, infections, toxins, diabetes, and cardiovascular diseases.[1] When biological triggers are present, they activate our innate immune system within minutes and the immune system secretes signals to communicate a coordinated response.[2,3] However, our immune response differs individually due to various conditions of stress, epigenetics, age, existing medical conditions, and disease state. This is evident in the case of sepsis where the leading cause of death is an overexuberant dysfunctional immune response affecting mostly elderly patients with preexisting medical conditions.[4] Thus, profiling the innate immune response remains vital in elucidating immune state, disease pathogenesis, and clinical risk stratification.

Current immune profiling techniques using microfluidic integrated fluorescence-activated cell profiling,[5] enzyme-linked immuno sandwiched assay (ELISA),[6,7] and single-cell gene sequencing focus primarily on cytokines and cluster of differentiation (CD) immune-cell surface markers.[8,9] These immune profiling methods require some form of blood preprocessing steps such as sample dilution, antibody labeling, and blood lysis centrifugation, which alters the native immune-cell activity convoluting the immune profiling.[10−12] The CD surface marker profiling and current cytokine assays alone do not correlate well with immune response and clinical outcomes due to the complex secondary pro- and anti-inflammatory effects.[13,14] New gene sequencing technologies enable the study of genetics at a single-cell level, resulting in rich database and information on immune responses in disease pathophysiology.[15] However, gene sequencing is an upstream static cellular process, while innate immune response is a downstream active and reactionary process.
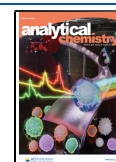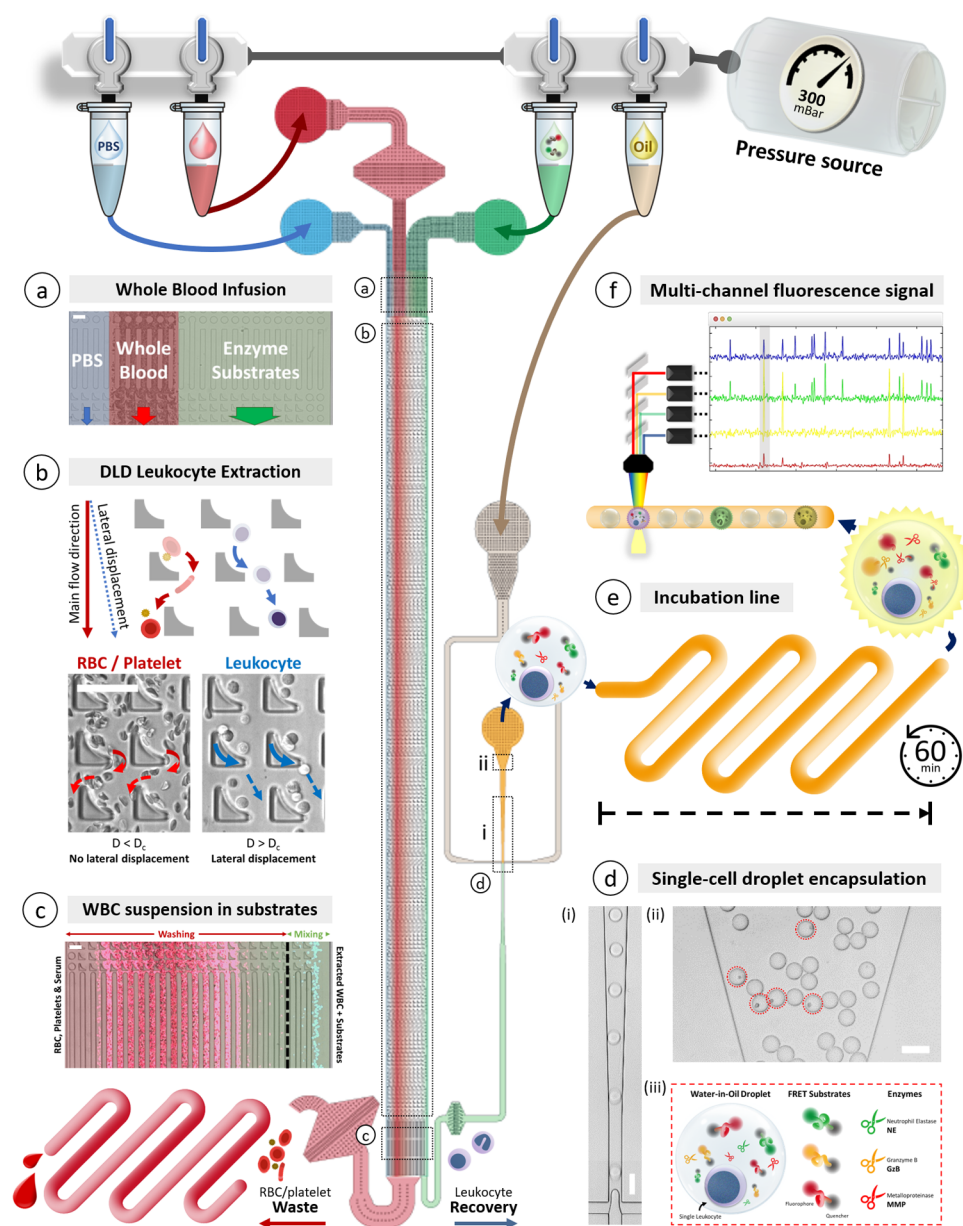
**Figure 1.** Schematics of the integrated microfluidic design comprising the DLD whole-blood processor and single-cell droplet assay. (a) Infusion filters and channels, (b) DLD leukocyte extraction array, (c) outlet bifurcation, (d) single-cell droplets, (e) incubation line, and (f) multichannel fluorescence signal from cleaved substrates. The system is operated in continuous-flow mode controlled by a customized pressure manifold. Scale bars represent 50 $\mu$m.

Enzymatic secretions of immune cells are fundamentally linked to the immune-cell functions as these secreted biomolecules are pivotal to the direct activity of inflammation,[16] cell migration,[17] signaling,[18] and cytotoxic activity.[19] Compared to cytokines and CD markers, these biomolecules and their associated pathways are relatively poorly mapped. Metalloproteinase is a large class of enzymes that immune cells secrete for interstitial migration and inflammatory signaling;[20] elastase is commonly secreted by neutrophils and monocytes with bactericidal properties and participates in cytokine induction;[21] and granzymes are known to be secreted from cytotoxic T-cells and natural killer cell granules, which trigger cell signaling and death.[22] Enzymatic secretions of immune cells are, therefore, direct indicators of clinical immune response and activity. The detection of these secreted biomolecules is generally performed in bulk plasma analysis,

and single-cell studies remain challenging to be conducted due to the need of complex sample preprocessing, single-cell isolation, and ELISA protocols.[23,24] Critically, current ELISA-based immune assay measures the presence of the protein that might not be a functional enzyme.

Our approach here eliminates the aforementioned challenges by developing a fully integrated microfluidic chip for multiplexed profiling of native immune single-cell enzyme secretion from 50 $\mu$L of undiluted blood. With a total analysis time of 60 min, the integrated platform performs six tasks of leukocyte extraction, cell washing, fluorescent enzyme substrate mixing, single-cell droplet making, droplet incubation, and real-time readout for leukocyte secretion profiling of neutrophil elastase (NE), granzyme B (GzB), and metalloproteinase (MMP). The device features an unconventional deterministic lateral displacement (DLD) L-shaped pillar
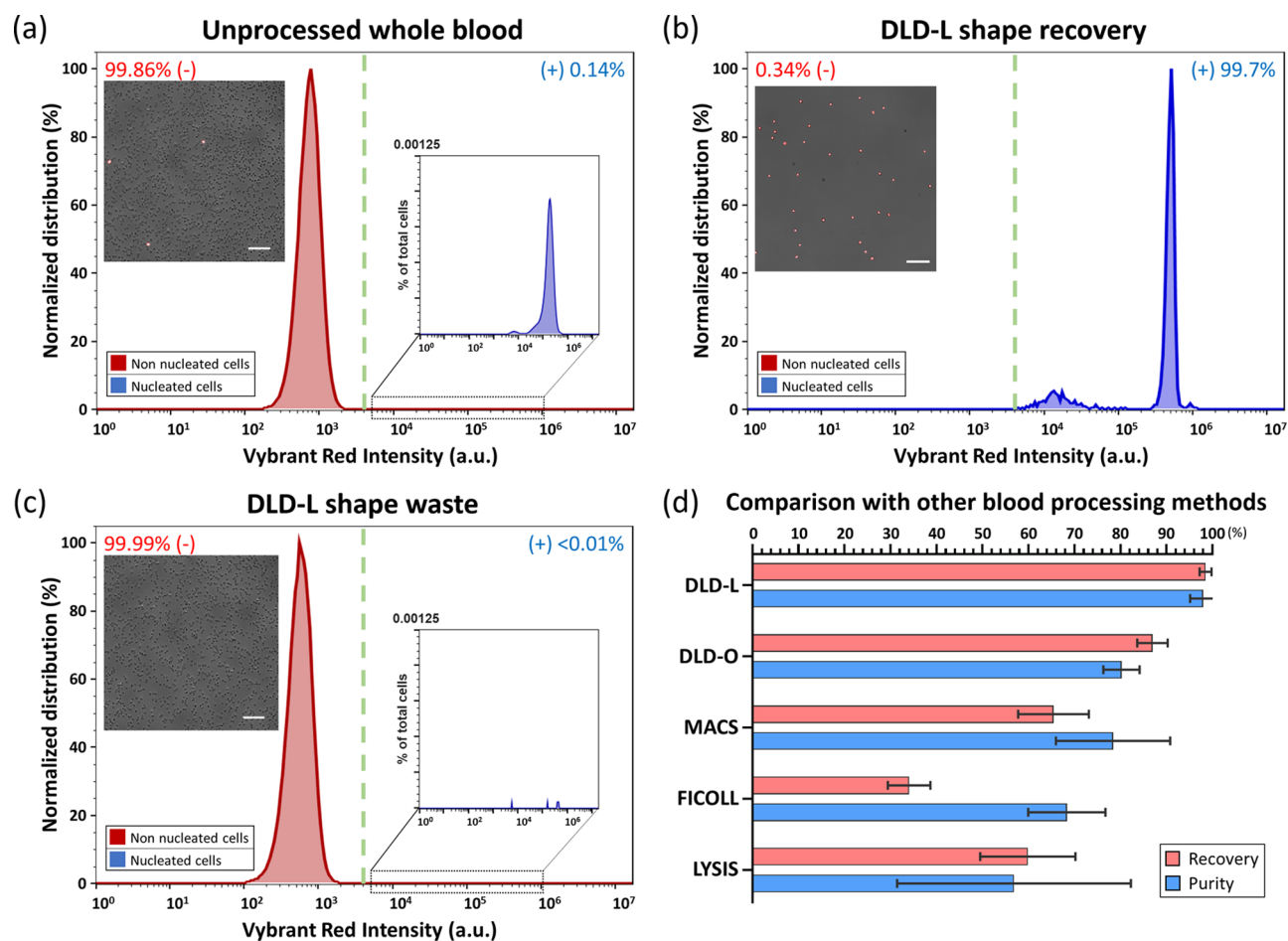
**Figure 2.** Characterization of DLD whole blood processor's leukocyte extraction efficiency and comparison with existing methods. (a) Normalized FACS histogram of original whole blood sample based on 300 000 events. The inset shows the magnified view of the gated region (green dotted line) with the Vybrant Red DNA dye, which stains the cell nucleus in whole blood. RBCs with no nucleus are not stained and lie on the left-hand side of the gating. The numbers at the top corners represent the population proportion of each gated group. (b) FACS histogram based on at least 3000 events of the leukocyte sorted using the DLD-L specifications. The waste outlet of the sorting is shown in (c) with a similar inset showing the magnified view of the gated region based on Vybrant Red DNA dye. All microscope image insets include a false-color bright-field overlay of DNA Vybrant Red fluorescence images. The scale bar indicates 100 $\mu$m. (d) Bar plot comparison of leukocyte recovery and purity from whole blood using DLD L-shape, DLD O-shape, Ficoll gradient centrifuge, RBC lysis, and magnetic activation cell sorting (MACS). The error bars represent the standard deviation of $n = 3$ samples used for the plots.

design capable of achieving >98% recovery and >99% purity of leukocytes from whole blood at a high throughput of ~6 million blood cells (1.5 $\mu$L of whole blood) per minute. The assay from blood to single-cell multiplex enzymatic profiling is performed in a continuous flow without the need for primary or secondary antibody labeling, blood lysis, or centrifuge washing steps.

### ■ EXPERIMENTAL SECTION

A fully integrated single-cell droplet profiling system was designed and fabricated for this study. The system schematics shown in Figure 1a−f perform six functions of whole blood sample infusion, leukocyte extraction, mixing of cells with enzymatic substrate fluorescent probes, isolation of single-cell reaction droplet, incubating the cells with the enzyme Förster resonance energy transfer (FRET) substrates, and finally detecting the secreted enzymes profiles based on the fluorescent detection using photomultiplier tubes (PMTs) for four fluorescent excitation and emission channels (Supporting Information 1).

The integrated system consists of four pressurized inlets for sample buffer, whole-blood sample, washing buffer comprising enzyme fluorescence substrates neutrophil elastase (NE), granzyme B (GZB), and metalloproteinase (MMP) FRET substrates to be used for the immune profiling, and finally oil with surfactant to enable stable droplet formation. The two outlet channels are red blood cells (RBC) waste outlets and the droplets outlet containing leukocytes encapsulated with FRET substrates, which will be cleaved in the presence of secreted enzymes from the individual immune cells (Figure 1d). These droplets will transit into an incubation tube and are finally injected into the microfluidic observation window for single-droplet fluorescent measurement (Figure 1e,f and Supporting Information 1).

**Comparison of Whole-Blood Processing Efficiency.** Freshly drawn whole blood was injected into the device at a rate of ~1.5 $\mu$L/min at 300 mbar, and the sorted leukocyte region is colored blue (Figure 1a). The fluorescence-activated cell sorting (FACS) panel staining was conducted with 0.6 $\mu$L of Vybrant Red DyeCycle Ruby Stain (Thermo Fisher Scientific, Singapore) added to each milliliter of sample. A

(a)

(b)
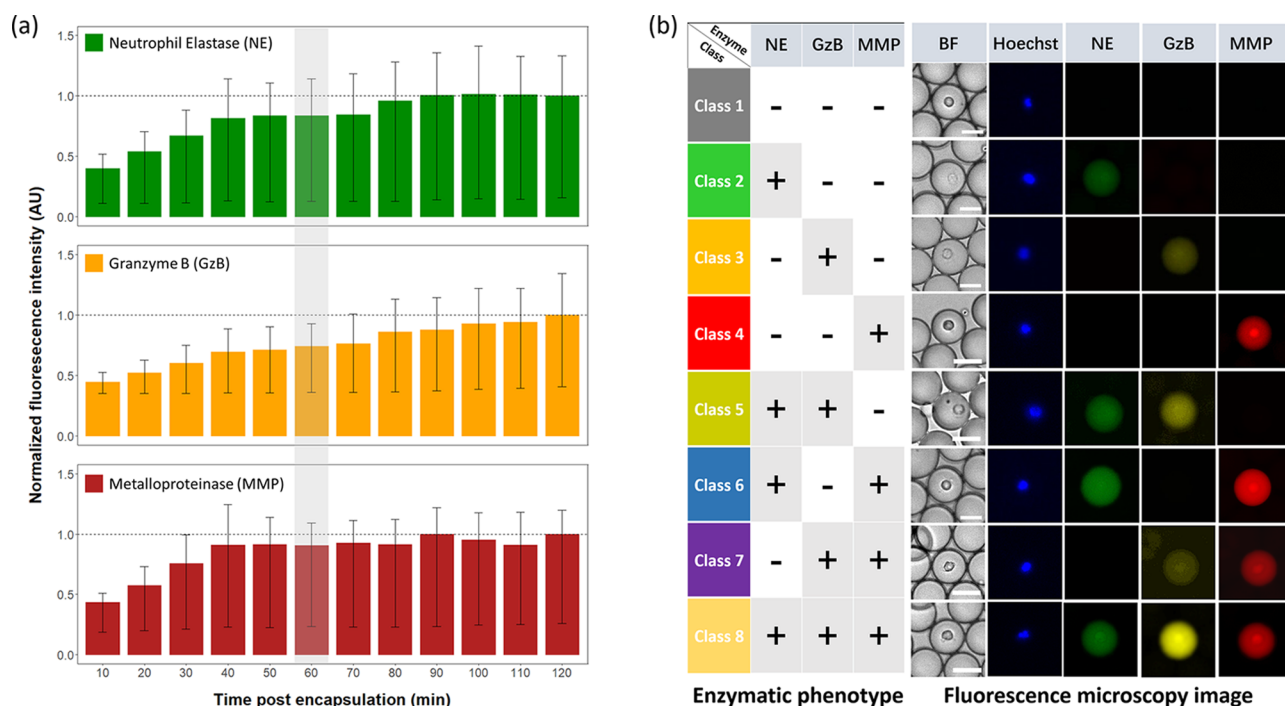


**Figure 3.** Characterization of single-cell droplet enzymatic substrate fluorescence measurements. Individual images of single-cell droplets were captured for bright-field image, Hoechst (blue channel), NE (green channel), GzB (yellow channel), and MMP (red channel). Fluorescence intensities from substrate channels were traced from 239 single leukocyte droplets, over a period of 120 min with a 10 min interval. Mean fluorescence intensity of each time point was normalized against the value at 120 min and represented in (a). Error bars show the 25th quantile (bottom) and 75th quantile (top) of fluorescence level within all single-cell droplets. A total of eight different enzyme expression and phenotype combinations were captured and displayed in (b), where colored fluorescence images of the various fluorescence channels were captured to show subpopulation representation of each phenotype. The bright-field images show the droplet with the captured cell with the scale bar denoting 25 μm.

stained control was prepared for each blood source by mixing 50 μL of whole blood with the Vybrant Red dye, while a negative control was prepared without addition of Vybrant Red. Both control samples were then diluted 1:4000 in 1× phosphate-buffered saline (PBS) and counted for a total of 300 000 events in FACS. The outputs from each WBC recovery method were labeled as either Recovery or Waste (Figure 2). The recovery portion and waste portion of each method were stained with Vybrant Red and diluted accordingly for the optimal concentration for FACS (Supporting Information 2).

**Single Leukocyte Enzyme Secretion Time Lapse Study.** The FRET substrates used in this project are: neutrophil elastase substrate ((Z-AAAA)2Rh110 Abs/Em:497/520 nm, Anaspec), Granzyme B substrate (5TAMRA-VGPDFGR-K(QSY7)-NH2 Abs/Em: 546/580, CPC scientific), and metalloproteinase substrate (QSY21-HGDQMAQKSK(Cy5)-NH2 Abs/Em:649/666 nm, CPC Scientific). The lyophilized substrates were dissolved in dimethyl sulfoxide (DMSO) at a concentration of 5 mM, and the assay cocktail was prepared as 5 μM of each substrate in 1× PBS. Bovine serum albumin (BSA, 1%) was added into the cocktail to facilitate the dissolution of substrates. Hoechst 33342 was added to all groups before chip processing. Droplets generated within the first 5 min of whole blood processing were collected and immediately reinjected to a poly-(dimethylsiloxane) (PDMS)-made visualization chamber (30 μm height). The first time point was recorded at 10 min from the start of sample collection. Fluorescence images representing signal from all three substrates were taken with a Leica

DMi8 fluorescence microscope every 10 min up to 120 min. Total fluorescence intensity for each cell-containing droplet was calculated and normalized against signal from the droplet containing fully cleaved substrates.

**Continuous-Flow Profiling of Leukocytes from Whole Blood.** A 50 μL aliquot of whole blood sample from each blood donor was premixed with Hoechst 33342 DNA stain (Sigma, Singapore) at the recommended working concentration. Donor recruitment criteria are elaborated in Supporting Information 3 with patients recruited from participants of the Nephropathy In Congestive Heart Failure and Biomarker Evaluation-Exemplification (NICHE2) study (DSRB Reg: 2016/00193). After the blood was transferred to the inlet of the microfluidic device, positive pressure was generated in the air chamber to initialize blood processing. Pressure was kept almost constantly at around 300 mbar throughout each experiment, which maintained droplet generation rate, single-cell encapsulation rate, and droplet size at a constant level (Supporting Information 4). Single leukocyte droplets were collected for 5 min; then, infusion of the blood sample was stopped by blocking its input pressure. Meanwhile, continuous fluid flow pushed the droplets through a 2.1 m Ø0.38 mm incubation tubing (Scientific Commodities, Inc.). The length of tubing was calculated to achieve ~60 min transit time before the droplets reach the fluorescence detection area (Supporting Information 1). A tubing of identical length was attached to the RBC outlet for resistance balancing. All videos of droplet generation and leukocyte particle tracking were captured using a Phantom v7.1 high-speed camera. Single-cell secretion data
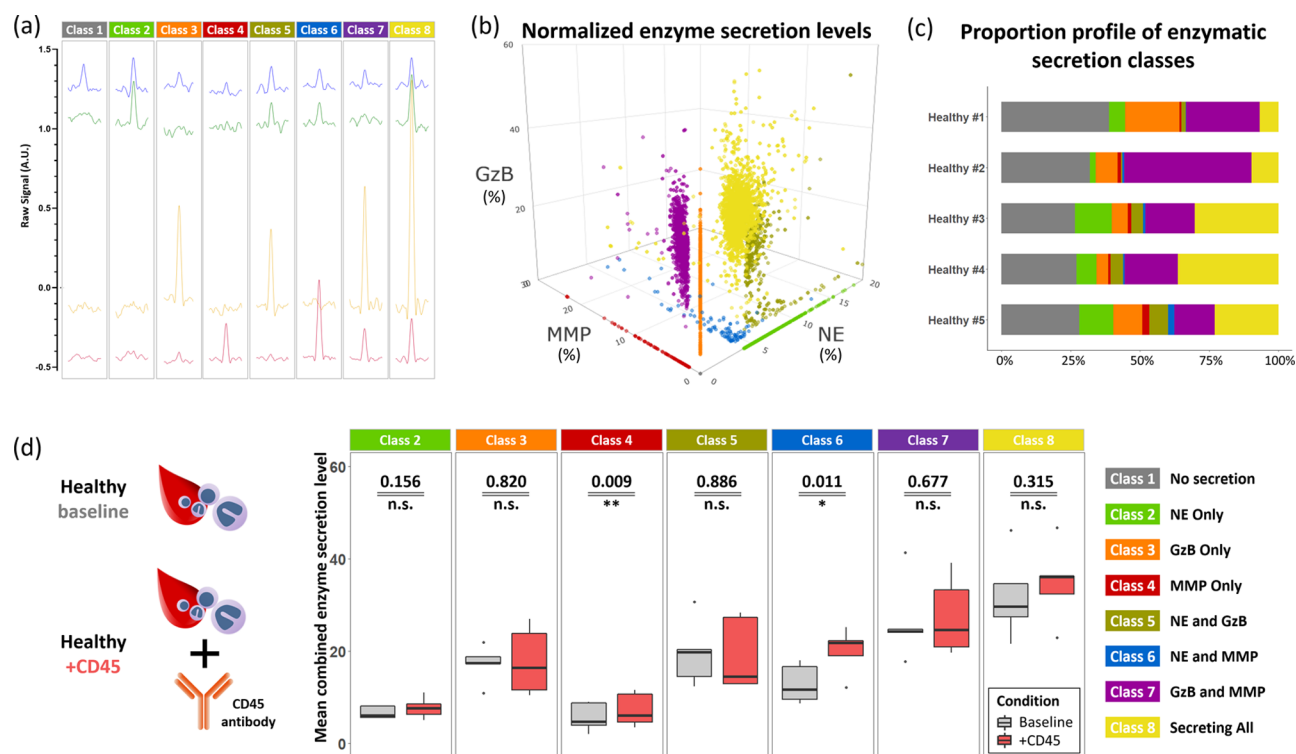
**Figure 4.** Continuous-flow profiling leukocytes from healthy donors. (a) Raw single-cell droplet peak signal from all four PMT channels in real-time representing channels to probe for Hoechst stained cells (blue), NE (green), GzB (orange), and MMP (red). (b) 3D visualization of the leukocyte enzymatic secretion profile of a healthy donor. The eight enzymatic classes were denoted in different colors (class 1 not shown in the figure). (c) Proportion profiles of eight enzymatic classes for five healthy donors. (d) Specific class enzyme secretion levels from healthy donors and healthy donors sample spiked with CD45 antibody, a standard leukocyte surface marker label for $n = 5$ samples. A paired two-tailed $t$-test analysis was performed, with * and ** denoting $p < 0.05$ and $p < 0.01$, respectively.

were analyzed from PMT signals using custom Matlab functions (Supporting Information 5).

## RESULTS AND DISCUSSION

**Leukocyte Extraction from Whole Blood.** Effective sorting of leukocytes is needed to enable single-cell enzyme profiling. DLD devices have shown potential for effective sorting of exosomes, RBC, leukocytes, cancer cells, and stem cells.[25,26] Both "I"- and "L"-shape DLD pillars showed enhanced RBC sorting efficiency compared to conventional round pillar structures with the same DLD specification.[27,28] Compared to the I-shaped pillar, the L-shaped pillar results in a lower device resistivity (Supporting Information 6), and as leukocytes are deformable, DLD-L is hypothesized to be effective for leukocytes sorting.[29] Thus, we evaluate the sorting efficiency of the DLD system designed with a cutoff sorting size of 5.5 $\mu$m comprising unconventional L-shaped DLD structures (DLD-L) (Figure 1b and Videos S1 and S2). The DLD-L sorting resulted in a recovered leukocyte purity of 99.7%, while most of the leukocytes were depleted in the RBC waste outlet (Figure 2a–c). This equates to an approximately 700-fold enrichment of leukocytes. When both DLD-L and conventional circular pillar DLD (DLD-O) are designed for the same cutoff size (5.5 $\mu$m), the former achieved better recovery efficiency and better purity than the latter (Figure 2d and Supporting Information 7), which enable complete WBC profiling from whole blood.

For effective sorting of leukocytes using DLD-O structures, a theoretical cutoff size of 4.0 $\mu$m is required for ~97% leukocyte recovery.[30] In comparison, our DLD-L design matched the

recovery performance at a $D_c$ of 5.5 $\mu$m. This translates to a proportionally smaller device, larger gaps (less clogged device), and lower channel resistance.

In addition, we compared the sorting efficiency of DLD-L with other established whole blood leukocyte extraction methods, including blood lysis, MACS sorting, and Ficoll separation, using the same protocol (Supporting Information 2). As summarized in Figure 2d, our DLD-L design had the highest average leukocyte recovery efficiency of 98.6% among the compared methods. This sorting performance is a significant improvement on the previous work by Jing et al., which could recover 60% of leukocytes from lysed blood sample with a DLD size cutoff of 7.0 $\mu$m.[31] Apart from enhanced sorting utility, the DLD-L whole blood processor also integrates many other functions. The DLD array directs leukocytes to a media containing the buffers and reagents required for downstream droplet assays, where serum is blocked off by diffusion-limited laminar co-flow.[31] This method of sorting, washing, and complete resuspension in the new buffer within a single setup replaces the need for cell lysis, centrifugation, and multiple cell handling steps.

**Single-Cell Enzymatic Heterogeneity.** The sorted leukocytes flow into a region of the device shown in Figure 3a where oil is injected as a crossflow to break the surface tension of the aqueous phase containing sorted leukocytes into homogeneous droplets of 28 $\mu$m diameter (Supporting Information 4 and Video S3). Three enzymatic fluorescent FRET peptide substrates for NE,[32] GzB,[33] and MMP[5,34] were used to probe the immune single-cell secretion within the droplet reaction (Figure 1d). A total of 239 droplets were
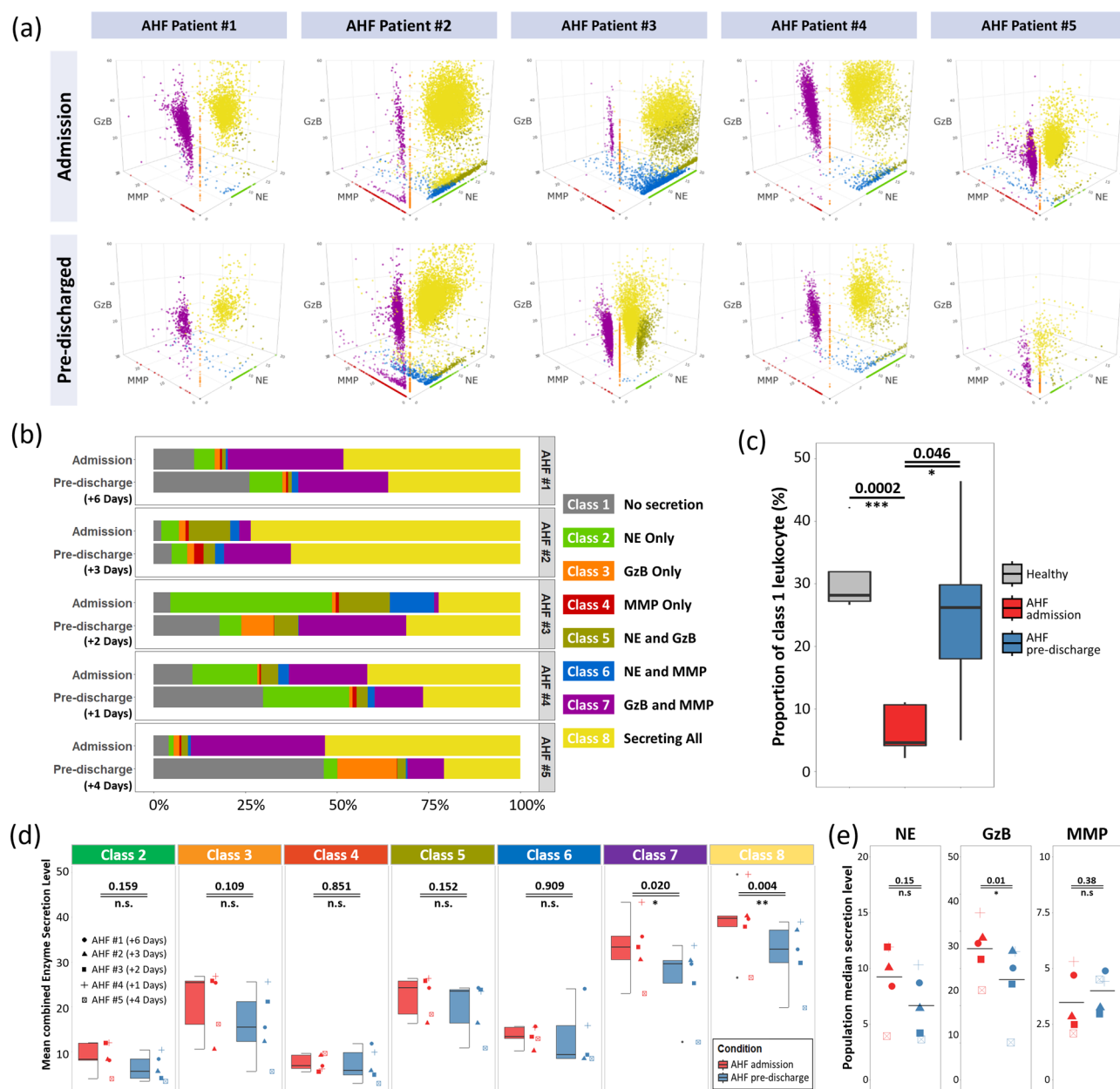
**Figure 5.** Single-cell leukocyte enzymatic profiling of acute heart failure (AHF) patients at hospital admission and predischarge. (a) Leukocyte single-cell enzyme secretion 3D plot distribution of AHF patient whole blood samples collected at admission day (top row) and predischarge day (bottom row), based on the leukocyte secretion of NE, GzB, and MMP. (b) Proportion profiles of the eight classes of enzyme activity for admission and predischarge immune profiles for the AHF patients. (c) Comparison of class 1 (no secretion) leukocyte between five healthy donors and five AHF patients (admission and predischarge). (d) Box plot of mean combined enzyme secretion level showing the differences in enzyme expression levels for all eight classes among AHF patients. (e) Comparison of population median secretion level of individual enzyme for admission AHF patients and AHF patients. For all $t$-tests in (c−e), single line indicates two-tailed unpaired $t$-test assuming unequal variance, whereas double line indicates two-tailed paired $t$-test. The asterisks *, **, and *** signify $p < 0.05$, $p < 0.01$, and $p < 0.001$, respectively.

tracked over time, and the plots show that the mean normalized intensity seems to plateau at around 80 min for NE, 120 min for GzB, and 50 min for MMP (Figure 3a). Thus, a suitable timing for measurement would be at 60 min incubation time, where NE, GzB, and MMP mean fluorescence signals reach ~85, 75, and 90% maximum fluorescent intensities, respectively.

The background signals of empty droplets are low, which is the advantage of integrated cell prewashing steps.[31] This removes the presence of any background enzymes in the blood serum. We were able to see distinct differences between each

droplet for the various fluorescent channels categorized into eight classes shown in Figure 3b. The heterogeneity of single-cell secretions is evident with the 8 different combinations of secretion profiles. This is intriguing as it is conventionally known that granzyme B is generally secreted by leukocytes during cytotoxic events while neutrophil elastase is secreted by neutrophils. A possible explanation for the heterogeneous observations is that there are other lesser-known secreted enzymes that contribute to nonspecific fluorescent probe cleavage.[35] For instance, granzymes are a family of homologous serine proteases that includes six different human granzymes

(A/B/H/K/M) while only granzymes A and B are well studied and commonly profiled.[36] T-cells also express elastase albeit a slightly different variation from neutrophil elastase.[37] The experiments highlight specific enzymatic secretion phenotypes of basal functional activities between the immune population. It is important to note that what we are profiling here is not a CD marker phenotype but the immune-cell functional phenotype by enzymatic secretion.

**Continuous-Flow Enzyme Profiling.** To enable continuous-flow testing, the droplets generated by the microfluidic device are injected into an incubation tube to enable at least 60 min of incubation. This method of single-cell droplet incubation via tubing droplet feed delay was first introduced by Ng et al.[5] The integration complements the highly efficient leukocyte sorting performance of the DLD-L component, enabling our system to capture a pan leukocyte population profile in a label-free manner. This is different from common immune profiling practices that start from peripheral mononuclear blood cells (PMBC) only.[38,39]

Figure 4 shows the data from continuous profiling using the integrated PMT and microfluidic setup, where the fluorescence signals from droplets were detected as peak electrical signals and converted into single-cell enzymatic secretion profiles. Figure 4a displays the raw single-cell signal representing eight enzyme secretion classes of all possible combinations of NE, GzB, and MMP secretion phenotypes. Hoechst was detected synchronously with fluorescence from cleaved FRET substrates to identify droplets containing single nucleated cell. The single-cell enzyme secretion level was then obtained by normalizing the signal to the maximum fluorescence yield of individual channels. The eight enzyme secretion classes of leukocytes clustered at distinct positions in the three-dimensional (3D) scatter chart due to various distinct secretion profiles of NE, GzB, and MMP (Figure 4b). These eight classes of immune-cell enzyme secretion phenotypes are not detectable in conventional bulk plasma enzyme assays, which would quantify the bulk activities of each enzyme. Each enzyme secretion class constituted different proportions in the total leukocyte population as well (Figure 4c). We profiled a total of five healthy donors, among which at least 25% of the leukocytes were in class 1 (no enzyme secretion). Class 7 (GzB and MMP) and class 8 (secrete all enzymes) were the next largest contributor to the enzymatic profiles of these healthy donors. Donor-to-donor heterogeneity is evident in these profiles, and understanding these differences could lead to personalized immune profiling.

Since immune-cell response sensitivity to external triggers and CD45 is a co-receptor that is related to leukocyte activation,[40,41] we tested whether labeling whole blood sample with CD45 would change the leukocyte enzyme secretion profile of these healthy donors (Figure 5d and Supporting Information 8). We define mean combined enzyme secretion level to measure the mean intensity of enzyme secretion level for individual classes. In particular, class 4 (MMP only) and class 6 (NE and MMP) cells responded more actively to CD45 labeling than other classes. Gao et al. reported that the cross-linking CD45 activates neutrophils and promotes secretion of IL-6, which is strongly correlated to the release of gelatinase and specific granules.[41,42] Our unconventional enzyme secretion-based immune classification method may inspire new insights into selective immune-cell degranulation initiated by surrounding triggers, as the specific surface markers corresponding to such an event have yet been extensively

characterized for all peripheral leukocytes, especially for non-PMBCs.[43]

**Patient-Specific Immune Enzymatic Profile.** Inflammatory biomarkers are important diagnostic and prognostic probes for acute heart failure (AHF) as both inflammation and heart failure are strongly interconnected and mutually reinforcing. Secreted enzymes of leukocyte are strongly correlated with AHF inflammatory biomarkers, as they play key functional roles during inflammation and tissue remodeling.[44] NE is associated with neutrophil activation and adhesion during ischemia-reperfusion inflammation;[45,46] GzB is a key mediator of cytotoxic T lymphocyte-induced apoptosis;[47] and MMP is related to extracellular matrix extravasation and ventricular remodeling.[48,49] Here, we applied our system to profile peripheral blood from five different AHF patients on admission day and predischarge day, which serves as a preliminary test to study single-cell leukocyte enzymatic secretion profiles of NE, GzB, and MMP in AHF.

Interpatient heterogeneity is seen on both admission profiles and predischarge profiles. Each patient had a unique set of cluster positions of the eight enzyme secretion classes in the 3D plot defined by the level of NE GzB and MMP (Figure 5a) and a unique pattern of class proportion determined by distribution of enzymatic phenotypes across the entire leukocyte population (Figure 5b). The variability among AHF patients could be attributed and not limited to AHF severity, comorbidities, immune response, medical treatment, and hospitalization duration.[50,51] This was reflected by our single-cell enzyme profiling result as different levels of change in cluster positions and proportions in admission and predischarge profiles.

Despite the presence of heterogeneity, we observed several trends between admission and predischarge AHF patients. First, the proportion of class 1 (no secretion) increased consistently from $6.5 \pm 3.6$ to $25.1 \pm 13.7\%$, $p = 0.046$ (Figure 5c and Supporting Information 9). As expected, AHF patients on admission day had a significantly lower class 1 cell proportion than healthy donors, whereas there was no significant difference between predischarge AHF patients and healthy donors (Figure 5c). Second, class 7 (GzB and MMP) and class 8 (secreting all three enzymes) leukocytes from AHF patients showed significantly elevated mean combined enzymatic secretion levels in admission profiles compared to predischarge profiles (class 7: $33.2 \pm 6.6$ to $26.2 \pm 7.5$, $p = 0.020$; class 8: $38.8 \pm 7.4$ to $31.7 \pm 6.7$, $p = 0.004$). Notably, class 8 leukocytes account for at least 20% of leukocyte population for each AHF patient (Figure 5b and Supporting Information 9). From the admission test to the predischarge test, the increase of class 1 proportion and the reduction of class 8 cell secretion jointly suggest immune activation immediately following AHF and resolution of post-AHF inflammation when the patients were cleared for discharge.

Among the three enzymes we tested, GzB showed a significant decrease in secretion level between admission and predischarge leukocyte population of every AHF patient (median: $35.3 \pm 6.9$ to $27.0 \pm 9.1$, $p = 0.010$, Figure 5e), which is consistent with existing bulk serum assay results.[47] However, our multienzyme combination profiling approach provides information beyond the value of individual or bulk serum NE, GzB, and MMP levels in AHF. Moreover, the unconventional enzyme phenotype classification reveals unique class proportion signatures that are comparable between admission and predischarge states, as seen for patients 1, 2,

and 4 in Figure 5b. It is important to note that admission and predischarge profiling tests were independently performed between 1 and 6 days apart from each other. This is not only indicative of the consistency of our profiling method but also suggests that the immune signatures and responses are potentially patient-specific.

Collectively, we showed that label-free functional leukocyte assessment is potentially feasible in AHF and distinct enzymatic secretion profiles correlate to their clinical states. The variability in blood leukocyte enzyme secretomes may be prognostic for AHF as well. Future studies with long-term outcome data such as mortality and readmission rates of AHF patients are required to further investigate the distinct role of leukocyte from each enzymatic secretion class during the course of AHF.

## CONCLUSIONS

Single-cell enzyme secretomics play an important role in our innate and adaptive immune response. We have developed an integrated immune profiling platform to probe single-cell enzymatic secretome of NE, GzB, and MMP. The platform processes whole blood and reduces quantitative artifacts based on sample preprocessing protocols such as cell lysis or labeling. To our knowledge, this is the first platform to combine these three markers to profile the basal or native immune system at a single-cell resolution. We show that CD marker labeling of cells changes the enzyme secretion profile, highlighting the sensitivity of immune cells to external triggers or antibody binding events. Through the recruitment of AHF patients, we observed immune modulation for certain enzymatic activity phenotypes studied here and reduction in immune enzyme secretion, for predischarge patients. Finally, immune secretion profile of each patient showed evidence of patient-specific immune signatures with proportions of enzyme secretome activity conserved from admission to predischarge profiling. This platform opens opportunities to probe native and physiologically relevant immune-cell profiling, which bridges the current technological and medical gap in understanding immune response and biological triggers.

## ASSOCIATED CONTENT

### Supporting Information

The Supporting Information is available free of charge at https://pubs.acs.org/doi/10.1021/acs.analchem.0c03512.

> Device fabrication and experimental setup; FACS histogram plots for recovery data from whole blood leukocyte purification methods; patient recruitment criteria; characterization of pressure-driven integrated flow system; data processing protocol to convert raw PMT signal to single-cell enzyme secretion level; device resistivity simulation of I-shaped and L-shaped DLD structures; DLD design and specifications for L and O pillar shapes; single-cell secretion profile for healthy donors; and detailed enzymatic secretion class proportional profile of AHF patients (PDF)

> Infusion of whole unprocessed blood into the microfluidic device sandwiched between two buffer streams (Video S1) (MOV)

> Output sorted streams of RBC (left) and leukocytes (right) in DLD-L device (Video S2) (MOV)

> Single-droplet generation at a cross-junction showing droplets formed with two different pressures (Video S3) (MOV)

## AUTHOR INFORMATION

### Corresponding Authors

◆Kerwin Kwek Zeming — *Critical Analytics for Manufacturing of Personalised Medicine, Singapore–MIT Alliance for Research and Technology, 138602, Singapore;* orcid.org/0000-0002-3088-3604; Email: kerwin@smart.mit.edu

Shir Lynn Lim — *Department of Cardiology, National University Heart Center, 119228, Singapore; Yong Loo Lin School of Medicine, National University of Singapore, 117597, Singapore;* Email: shir_lynn_lim@nuhs.edu.sg

### Authors

◆Ri Lu — *Critical Analytics for Manufacturing of Personalised Medicine, Singapore–MIT Alliance for Research and Technology, 138602, Singapore; Graduate School for Integrative Sciences and Engineering, National University of Singapore, 119077, Singapore*

Kai Lee Woo — *Department of Cardiology, National University Heart Center, 119228, Singapore*

Guoyun Sun — *Graduate School for Integrative Sciences and Engineering, National University of Singapore, 119077, Singapore*

Kai Yun Quek — *Critical Analytics for Manufacturing of Personalised Medicine, Singapore–MIT Alliance for Research and Technology, 138602, Singapore*

Lih Feng Cheow — *Critical Analytics for Manufacturing of Personalised Medicine, Singapore–MIT Alliance for Research and Technology, 138602, Singapore; Graduate School for Integrative Sciences and Engineering and Department of Biomedical Engineering, National University of Singapore, 119077, Singapore*

Chia-Hung Chen — *Department of Biomedical Engineering, College of Engineering, City University of Hong Kong, Hong Kong;* orcid.org/0000-0002-4442-3203

Jongyoon Han — *Critical Analytics for Manufacturing of Personalised Medicine, Singapore–MIT Alliance for Research and Technology, 138602, Singapore; Department of Electrical Engineering and Department of Biological Engineering, Massachusetts Institute of Technology, Cambridge, Massachusetts 02142, United States*

Complete contact information is available at:
https://pubs.acs.org/10.1021/acs.analchem.0c03512

### Author Contributions

K.K.Z. and J.H. designed and fabricated the DLD integrated device. K.K.Z., S.L.L., and J.H. designed the clinical experiments. K.K.Z. and R.L. performed the experiments. C.-H.C., R.L., and G.S. developed and optimized the PMT systems and selected the enzyme substrates. S.L.L. applied for IRB and oversaw the clinical study. S.L.L. and K.L.W. recruited the patients and collected the samples. R.L. and K.Y.Q performed the WBC extraction methods with FACS analysis. R.L., G.S., and L.F.C. analyzed the PMT data and coded the algorithms for signal processing and visualization. K.K.Z., R.L., C.-H.C., S.L.L., and J.H. wrote the manuscript. All authors reviewed and approved the manuscript prior to submission.

## ■ REFERENCES

(1) Chaplin, D. D. *J. Allergy Clin. Immunol.* **2010**, *125*, S3.

(2) Boomer, J. S.; Green, J. M.; Hotchkiss, R. S. *Virulence* **2014**, *5*, 45.

(3) Leliefeld, P. H. C.; Koenderman, L.; Pillay, J. *Front. Immunol.* **2015**, *6*, No. 471.

(4) Zhou, F.; Yu, T.; Du, R.; Fan, G.; Liu, Y.; Liu, Z.; Xiang, J.; Wang, Y.; Song, B.; Gu, X.; Guan, L.; Wei, Y.; Li, H.; Wu, X.; Xu, J.; Tu, S.; Zhang, Y.; Chen, H.; Cao, B. *Lancet* **2020**, *395*, 1054.

(5) Ng, E. X.; Sun, G.; Wei, S.-C.; Miller, M. A.; DasGupta, R.; Lam, P. Y. P.; Chen, C.-H. *Anal. Chem.* **2019**, *91*, 1277.

(6) Junkin, M.; Kaestli, A. J.; Cheng, Z.; Jordi, C.; Albayrak, C.; Hoffmann, A.; Tay, S. *Cell Rep.* **2016**, *15*, 411.

(7) Zhou, Y.; Shao, N.; de Castro, R. B.; Zhang, P.; Ma, Y.; Liu, X.; Huang, F.; Wang, R.-F.; Qin, L. *Cell Rep.* **2020**, *31*, No. 107574.

(8) Landhuis, E. *Nature* **2018**, *557*, 595.

(9) An, X.; Sendra, V. G.; Liadi, I.; Ramesh, B.; Romain, G.; Haymaker, C.; Martinez-Paniagua, M.; Lu, Y.; Radvanyi, L. G.; Roysam, B.; Varadarajan, N. *PLoS One* **2017**, *12*, No. e0181904.

(10) Wu, L.; Guan, G.; Hou, H. W.; Bhagat, A. A. S.; Han, J. *Anal. Chem.* **2012**, *84*, 9324.

(11) Pitsillides, C. M.; Runnels, J. M.; Spencer, J. A.; Zhi, L.; Wu, M. X.; Lin, C. P. *Cytometry* **2011**, *79A*, 758.

(12) Vuorte, J.; Jansson, S. E.; Repo, H. *Cytometry* **2001**, *43*, 290.

(13) Monastero, R. N.; Pentyala, S. *Int. J. Inflammation* **2017**, *2017*, No. 4309485.

(14) Ecker, S.; Chen, L.; Pancaldi, V.; Bagger, F. O.; Fernández, J. M.; de Santa Pau, E. C.; Juan, D.; Mann, A. L.; Watt, S.; Casale, F. P.; Sidiropoulos, N.; Rapin, N.; Merkel, A.; Stunnenberg, H. G.; Stegle, O.; Frontini, M.; Downes, K.; Pastinen, T.; Kuijpers, T. W.; Rico, D.; Valencia, A.; Beck, S.; Soranzo, N.; Paul, D. S. *Genome Biol.* **2017**, *18*, No. 18.

(15) Singh, M.; Al-Eryani, G.; Carswell, S.; Ferguson, J. M.; Blackburn, J.; Barton, K.; Roden, D.; Luciani, F.; Giang Phan, T.; Junankar, S.; Jackson, K.; Goodnow, C. C.; Smith, M. A.; Swarbrick, A. *Nat. Commun.* **2019**, *10*, No. 3120.

(16) Fingleton, B. *Biochim. Biophys. Acta* **2017**, *1864*, 2036.

(17) Khandoga, A.; Kessler, J. S.; Hanschen, M.; Khandoga, A. G.; Burggraf, D.; Reichel, C.; Hamann, G. F.; Enders, G.; Krombach, F. *J. Leukocyte Biol.* **2006**, *79*, 1295.

(18) Devaney, J. M.; Greene, C. M.; Taggart, C. C.; Carroll, T. P.; O'Neill, S. J.; McElvaney, N. G. *FEBS Lett.* **2003**, *544*, 129.

(19) Peters, P. J.; Borst, J.; Oorschot, V.; Fukuda, M.; Krähenbühl, O.; Tschopp, J.; Slot, J. W.; Geuze, H. J. *J. Exp. Med.* **1991**, *173*, No. 1099.

(20) Manicone, A. M.; McGuire, J. K. *Semin. Cell Dev. Biol.* **2008**, *19*, 34.

(21) Pham, C. T. *Nat. Rev. Immunol.* **2006**, *6*, 541.

(22) Hiebert, P. R.; Granville, D. J. *Trends Mol. Med.* **2012**, *18*, 732.

(23) de la Rebière de Pouyade, G.; Franck, T.; Salciccia, A.; Deby-Dupont, G.; Grulke, S.; Heyden, L. V.; Sandersen, C.; Serteyn, D. *Vet. Immunol. Immunopathol.* **2010**, *135*, 282.

(24) Sedelies, K. A.; Sayers, T. J.; Edwards, K. M.; Chen, W.; Pellicci, D. G.; Godfrey, D. I.; Trapani, J. A. *J. Biol. Chem.* **2004**, *279*, 26581.

(25) Huang, L. R.; Cox, E. C.; Austin, R. H.; Sturm, J. C. *Science* **2004**, *304*, 987.

(26) Hochstetter, A.; Vernekar, R.; Austin, R. H.; Becker, H.; Beech, J. P.; Fedosov, D. A.; Gompper, G.; Kim, S.-C.; Smith, J. T.; Stolovitzky, G.; Tegenfeldt, J. O.; Wunsch, B. H.; Zeming, K. K.; Krüger, T.; Inglis, D. W. *ACS Nano* **2020**, *14*, 10784.

(27) Ranjan, S.; Zeming, K. K.; Jureen, R.; Fisher, D.; Zhang, Y. *Lab Chip* **2014**, *14*, 4250.

(28) Zeming, K. K.; Ranjan, S.; Zhang, Y. *Nat. Commun.* **2013**, *4*, No. 1625.

(29) Holmes, D.; Whyte, G.; Bailey, J.; Vergara-Irigaray, N.; Ekpenyong, A.; Guck, J.; Duke, T. *Interface Focus* **2014**, *4*, No. 20140011.

(30) Civin, C. I.; Ward, T.; Skelley, A. M.; Gandhi, K.; Peilun Lee, Z.; Dosier, C. R.; D'Silva, J. L.; Chen, Y.; Kim, M.; Moynihan, J.; Chen, X.; Aurich, L.; Gulnik, S.; Brittain, G. C.; Recktenwald, D. J.; Austin, R. H.; Sturm, J. C. *Cytometry, Part A* **2016**, *89*, 1073.

(31) Jing, T.; Lai, Z.; Wu, L.; Han, J.; Lim, C. T.; Chen, C.-H. *Anal. Chem.* **2016**, *88*, 11750.

(32) Jundi, B.; Ryu, H.; Lee, D.-H.; Abdulnour, R.-E. E.; Engstrom, B. D.; Duvall, M. G.; Higuera, A.; Pinilla-Vera, M.; Benson, M. E.; Lee, J.; Krishnamoorthy, N.; Baron, R. M.; Han, J.; Voldman, J.; Levy, B. D. *Nat. Biomed. Eng.* **2019**, *3*, 961.

(33) Choi, P. J.; Mitchison, T. J. *Proc. Natl. Acad. Sci. U.S.A.* **2013**, *110*, 6488.

(34) Ng, E. X.; Miller, M. A.; Jing, T.; Chen, C. H. *Biosens. Bioelectron.* **2016**, *81*, 408.

(35) Hochegger, K.; Eller, P.; Huber, J. M.; Bernhard, D.; Mayer, G.; Zlabinger, G. J.; Rosenkranz, A. R. *Immunology* **2007**, *121*, 166.

(36) Arias, M.; Martínez-Lostao, L.; Santiago, L.; Ferrandez, A.; Granville, D. J.; Pardo, J. *Trends Cancer* **2017**, *3*, 407.

(37) Bristow, C. L.; Lyford, L. K.; Stevens, D. P.; Flood, P. M. *Biochem. Biophys. Res. Commun.* **1991**, *181*, 232.

(38) Reyes, M.; Vickers, D.; Billman, K.; Eisenhaure, T.; Hoover, P.; Browne, E. P.; Rao, D. A.; Hacohen, N.; Blainey, P. C. *Sci. Adv.* **2019**, *5*, No. eaau9223.

(39) Goswami, S.; Walle, T.; Cornish, A. E.; Basu, S.; Anandhan, S.; Fernandez, I.; Vence, L.; Blando, J.; Zhao, H.; Yadav, S. S.; Ott, M.; Kong, L. Y.; Heimberger, A. B.; de Groot, J.; Sepesi, B.; Overman, M.; Kopetz, S.; Allison, J. P.; Pe'er, D.; Sharma, P. *Nat. Med.* **2020**, *26*, 39.

(40) Mitchell, G. B.; Khandaker, M. H.; Rahimpour, R.; Xu, L.; Lazarovits, A. I.; Pickering, J. G.; Suria, H.; Madrenas, J.; Pomerantz, D. K.; Feldman, R. D.; Kelvin, D. J. *Eur. J. Immunol.* **1999**, *29*, 1467.

(41) Gao, H.; Henderson, A.; Flynn, D. C.; Landreth, K. S.; Ericson, S. G. *Exp. Hematol.* **2000**, *28*, 1062.

(42) Naegelen, I.; Beaume, N.; Plançon, S.; Schenten, V.; Tschirhart, E. J.; Bréchard, S. *J. Immunol. Res.* **2015**, *2015*, No. 817038.

(43) Mollinedo, F. *Trends Immunol.* **2019**, *40*, 228.

(44) Van Linthout, S.; Tschöpe, C. *Curr. Heart Failure Rep.* **2017**, *14*, 251.

(45) Bell, D.; Jackson, M.; Nicoll, J. J.; Millar, A.; Dawes, J.; Muir, A. L. *Heart* **1990**, *63*, No. 82.

(46) Woodman, R. C.; Reinhardt, P. H.; Kanwar, S.; Johnston, F. L.; Kubes, P. *Blood* **1993**, *82*, No. 2188.

(47) Saito, Y.; Kondo, H.; Hojo, Y. *J. Cardiol.* **2011**, *57*, 141.

(48) Vuohelainen, V.; Raitoharju, E.; Levula, M.; Lehtimäki, T.; Pelto-Huikko, M.; Honkanen, T.; Huovila, A.; Paavonen, T.; Tarkka, M.; Mennander, A. *Scand. J. Clin. Lab. Invest.* **2011**, *71*, 553.

(49) Squire, I. B.; Evans, J.; Ng, L. L.; Loftus, I. M.; Thompson, M. M. *J. Card. Failure* **2004**, *10*, 328.

(50) Mentz, R. J.; Felker, G. M. *Heart Failure Clin.* **2013**, *9*, 359.

(51) Ahmad, T.; Lund, L. H.; Rao, P.; Ghosh, R.; Warier, P.; Vaccaro, B.; Dahlström, U.; O'Connor, C. M.; Felker, G. M.; Desai, N. R. *J. Am. Heart Assoc.* **2018**, *7*, No. e008081.